Electronic Supplementary Material (ESI) for ChemComm.

N,N'-bicarbazole-benzothiadiazole-based conjugated porous organic polymer for reactive oxygen species generation in live cells

Subhankar Kundu,[a] Biswajit Behera,[a‡] Arkaprabha Giri,[a‡] Nitu Saha[b] and Abhijit Patra[a]*

[a] Department of Chemistry, [b] Department of Biological Sciences,

Indian Institute of Science Education and Research Bhopal, Bhopal Bypass Road, Bhauri, Bhopal 462066, Madhya Pradesh, India

Email: abhijit@iiserb.ac.in

Contents

I. Instrumentation

1.1 Nuclear magnetic resonance (NMR) spectroscopy: Bruker Avance III NMR spectrometer of 500 and 126 MHz were used for the ^{1}H NMR and ^{13}C NMR analyses, respectively. The chemical shifts (δ) were reported in parts per million (ppm).

1.2 Fourier transform infrared spectroscopy (FTIR): A Perkin-Elmer Model 2000 FTIR instrument was used for the measurements. The samples were prepared in the form of pellets using KBr. The data was obtained through the averaging of the signals of twenty scans (resolution: 4 cm^{-1}) at ambient temperature.

1.3 Powder X-ray diffraction (PXRD): A PANalytical Empyrean X-ray diffraction instrument was employed for the PXRD experiment. The data was collected for the 2θ values ranging from 4 to 80 degrees.

1.4 Field emission scanning electron microscopy (FESEM): BCzBz dispersion in water was prepared through the sonication of the polymer dispersion (1 mg mL^{-1}) using a probe sonicator (frequency: 20 kHz, time: 30 s sonication with 5 s intervals continued for a total duration of 2 min). Then, the homogeneous dilute dispersion of BCzBz was drop-casted over a silicon wafer for the FESEM [Carl Zeiss (Ultraplus)] analysis.

1.5 High-resolution transmission electron microscopy (HRTEM): A homogeneous dilute dispersion of BCzBz polymer (in methanol, ultrasonication for 3 mins) was drop-casted onto a carbon-coated copper grid (400 mesh) for the TEM (FEI TALOS 200S at a working voltage of 200 kV) analysis.

1.6 Energy dispersive X-ray (EDX) spectroscopy: EDX was carried out at a working voltage of 200 kV using Cu as a reference.

1.7 Atomic force microscopy (AFM): AFM images of BCzBz dispersion drop-casted and dried over mica foil were captured using an Agilent 5500 AFM/SPM in tapping mode. The measurement was carried out using a silicon noncontact probe having a tip radius ~ 8 nm and force constant = 0.5 N m^{-1}.

1.8 Gas adsorption studies: The Quantachrome Autosorb QUA211011 equipment was used for the gas sorption measurements. N_2 gas adsorption-desorption measurements were carried out at 77 K to determine the surface area and the porosity. ASIQwin software was used to analyze all the isotherms. Degassing of the samples was carried out under a high vacuum using the same instrument for 24 h at 80 °C before the analysis. The pore size distribution was obtained analyzing the N_2 adsorption isotherms using the nonlocal density functional theory (NLDFT) method.

1.9 X-ray photoelectron spectroscopy (XPS):

XPS measurements were carried out using the PHI 5000 Versa Prob II, FIE Inc instrument. The core level scans were carried out with a scan time of 1 h per element.

1.10 Steady-state absorption spectroscopy: The UV-Visible absorption spectra were obtained through a Cary 100 spectrophotometer using 1 cm path length quartz cuvettes. The stray light was avoided during the measurements.

1.11 Cyclic voltammetry: Cyclic voltammetry (CV) was performed using a CH instrument. The three electrode-cell system was used for the measurement [working electrode: BCzBz-coated glassy carbon electrode; counter electrode: Pt wire; reference electrode: Ag/AgCl (KCl, 3M)]. Ferrocene-ferrocenium (Fc/Fc^+) was used as an internal standard. A scan rate of 100 mV/s was used. A solution of 0.1 (M) Bu_4NPF_6 in acetonitrile was used as the supporting electrolyte. 2 mg of BCzBz was well-dispersed in a binder solution of 25 wt% of polyvinylidene fluoride and 500 µL of ethanol through ultrasonication for 2 h to obtain a stable suspension. Then the pre-polished glassy carbon electrode was coated by 10 µL of the prepared dispersion. The electrode was dried for 1 h at 45 ℃ prior to the measurement.

1.12 Electron paramagnetic resonance (EPR): Bruker EMX MicroX spectrometer was used to record all the EPR spectra. The specific measurement details regarding reactive oxygen species (ROS) trapping are as following: the modulation frequency = 100 kHz, modulation amplitude = 0.2 G. The samples were prepared by adding 2,2,6,6-tetramethylpiperidine (TEMP) or 5,5-dimethyl-1-pyrroline *N*-oxide (DMPO) to toluene. Subsequently, BCzBz (2 mg) was added to the above solution.

1.13 Cell culture: The HeLa cells were grown in a Petri dish using media containing Dulbecco's modified Eagle's medium (DMEM), 2 mM L-glutamine, 1% penicillin-streptomycin, and 10% fetal bovine serum (FBS) under an atmosphere of 5% (v/v) CO_2 enriched air at 37 °C. Then the media was washed with phosphate-buffered saline (PBS). Cells were then taken for further experiments like cell viability assay and intracellular ROS detection.

1.14 Confocal laser scanning microscopy (CLSM): All the CLSM images were captured using a PicoQuant, MicroTime 200 instrument.

1.15 MTT assay: The cells were seeded in 96-well plates (Eppendorf) and incubated overnight before the treatment of aqueous dispersion of BCzBz polymer. The cytotoxicity of BCzBz polymer against HeLa cells can be calculated using equation S1.

$$\text{Cell Viability (\%)} = [(A_s - A_b) / (A_c - A_b)] \times 100\ \% \qquad \text{(S1)}$$

A_s, A_c, and A_b are the optical densities of the treatment group, control group, and blank well, respectively. Absorbance values were recorded at 570 nm using a SpectraMax i3x multi-mode microplate reader (Molecular Devices).

II. Synthesis & characterization

2.1 Chemicals: Chemicals were obtained in sufficient purity and were used directly unless stated otherwise. Carbazole (95%), *N*-bromosuccinimide (99%), potassium permanganate (99%), 2,1,3-benzothiadiazole-4,7- bis(boronic acid pinacol ester) (95%), dry toluene (99.8%), dimethyl sulfoxide (99%), 2′,7′-dichlorodihydrofluorescein diacetate (>97%), tetrakis(triphenylphosphine)palladium(0) (99.9%), 5,5-dimethyl-1-pyrroline *N*-oxide (97%), *N,N,N′,N′*-tetramethyl-*p*-phenylenediamine (97%), potassium carbonate (99%) tetrabutylammonium bromide (TBAB) (99%), potassium bromide (99%), tetrabutylammonium hexafluorophosphate (98%), poly(vinylidene fluoride), 2,2,6,6-tetramethylpiperidine (>99%), 1,3-diphenylisobenzofuran (97%), 1,2-diphenylethyne (98%), 4-chlorobenzenethiol (97%), were received from Sigma-Aldrich. All the cell culture media like DMEM, FBS, PBS were received from ThermoFisher Scientific. All spectroscopic grade solvents (n-hexane, toluene, chloroform, tetrahydrofuran, and dimethyl sulfoxide) were obtained from Spectrochem.

2.2 Synthesis and characterization of 3,3',6,6'-tetrabromo-*N,N′*-bicarbazole: To a solution of carbazole (3 mmol) in 5 mL DMF, *N*-bromosuccinimide solution (NBS, 1.5 mmol in 5 mL DMF) was slowly added while stirring for 4 h in an ice bath. Then, the reaction mixture was poured into ice-cold water. The mixture was then filtered to collect the crude white product. The product was recrystallized from EtOH/H_2O to get white crystals of 3,6-dibromo-9*H*-carbazole (yield 59 %, Scheme S1).

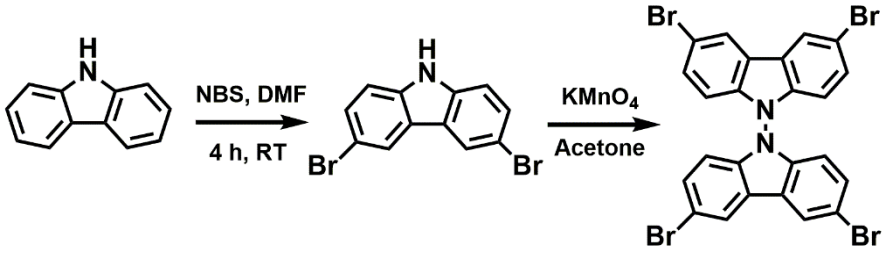

Scheme S1 Synthesis scheme of 3,3′,6,6′-tetrabromo-*N,N′*-bicarbazole.

^{1}H NMR (500 MHz, DMSO-d_6) δ_H (ppm): 11.58 (s, 1H), 8.42 (s, 2H), 7.52 (d, 2H), 7.46 (d, 2H).

^{13}C NMR (126 MHz, DMSO- d_6) δ_C (ppm): 111.23, 113.45, 123.56, 123.62, 128.97, 139.04.

The solution of 3,6-dibromo-9*H*-carbazole (0.62 mmol) and $KMnO_4$ (1.86 mmol) in acetone was refluxed at 65°C for 6 h. Then the reaction mixture was brought to room temperature. The solvent was evaporated under reduced pressure and the residue was suspended in chloroform. The filtrate was then washed several times with saturated aqueous $Na_2S_2O_3$ solution, brine, and then dried over $MgSO_4$. The filtrate was concentrated under reduced pressure. The residue was

recrystallized in a chloroform/hexane binary solvent mixture to get a colorless powder (yield 63 %, Scheme S1).

^{1}H NMR (500 MHz, DMSO-d_6) δ_H (ppm): 8.7 (d, 4H), 7.54 (dd, 4H), 6.89 (d, 4H).

^{13}C NMR (126 MHz, DMSO-d_6) δ_C (ppm): 138.11, 130.07, 124.31, 122.34, 113.95, 110.66.

2.3 Fabrication of conjugated porous organic polymer (BCzBz): 3,3',6,6'-tetrabromo-*N,N'*-bicarbazole (BCz, 0.23 mmol), 2,1,3-benzothiadiazole-4,7-bis(boronic acid pinacol ester) (Bz, 0.46 mmol), tetrakis(triphenylphosphine)palladium(0), tetrabutylammonium bromide (TBAB), 2 mL of degassed potassium carbonate (2 M) solution and 10 mL of dry toluene were taken in a 100 mL Schlenk tube. The reaction mixture was subjected to freeze-pump-thaw cycles to remove the dissolved oxygen after which it was stirred in an argon atmosphere at 110 °C for 48 h. Finally, the reaction mixture was poured into acidified cold methanol after bringing it to room temperature and was stirred for 30 min before filtration. The residue was washed several times using THF, methanol, and chloroform. Then Soxhlet extraction was carried out to wash the network polymer with methanol and chloroform each for 24 h and it was then dried under vacuum to obtain BCzBz (Fig. 1; brownish-orange; yield ~ 80%).

2.4 Optimization of polymerization conditions: The synthesis of BCzBz was performed using the above procedure in three different solvents, THF (60 °C), DMF (150 °C), and toluene (110 °C). BCzBz synthesized in toluene exhibited a surface area of 363 ± 33 m^2 g^{-1} with high porosity and was used in the present study (Table S1).

Table S1 Optimization of reaction conditions based on BET surface area values.

Entry	Solvent	Temperature (°C)	Surface area (m^2 g^{-1})	Remarks
1	THF	60	36	Less dispersed
2	DMF	150	98	Less dispersed
3	Toluene	110	396, 331	Highly dispersed

2.5 Characterization of BCzBz:

2.5.1 Stability of BCzBz dispersion: The brownish-orange BCzBz polymer was insoluble in organic solvents. However, it could be processed in the form of stable dispersion in multiple solvents like DMSO, toluene, and water (Fig. S1). The aqueous dispersion of BCzBz polymer was stable even after 24 h (Fig. S1b, c).

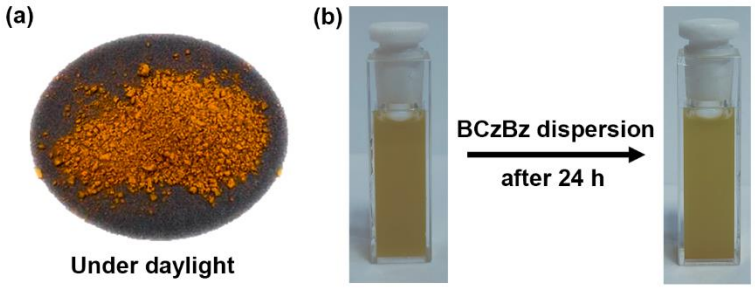

Fig. S1 Digital photographs of (a) BCzBz polymer. (b) The aqueous dispersion of BCzBz (1 mg mL^{-1}) under daylight depicting the stability of the dispersion.

2.5.2 Solid-state ^{13}C NMR analysis:

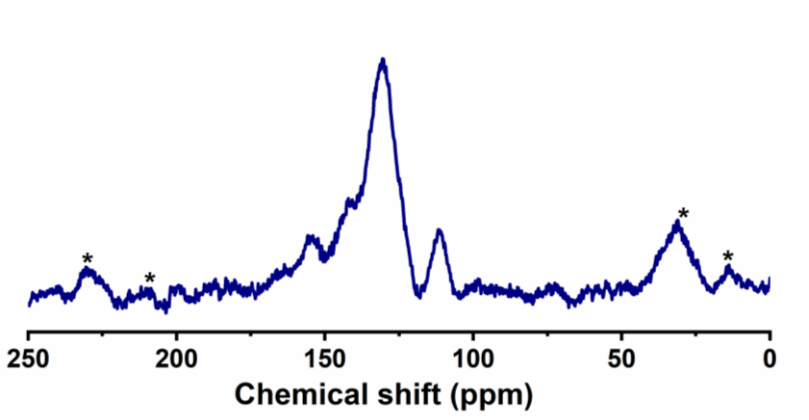

Fig. S2 Solid-state ^{13}C NMR of BCzBz at room temperature; *represents the spinning sidebands.

In the solid-state ^{13}C cross-polarization magic angle spinning (CP/MAS) NMR spectrum, the peaks resonated at 105 to 160 ppm designated for the aromatic carbons present in the polymer. The peak at 153 ppm originated from the C=N of the benzothiadiazole moiety. The peak at 25-50 ppm could be due to the spinning sidebands along with the unreacted boronic ester end groups (Fig. S2).

2.5.3 X-ray photoelectron spectroscopy (XPS) analysis:

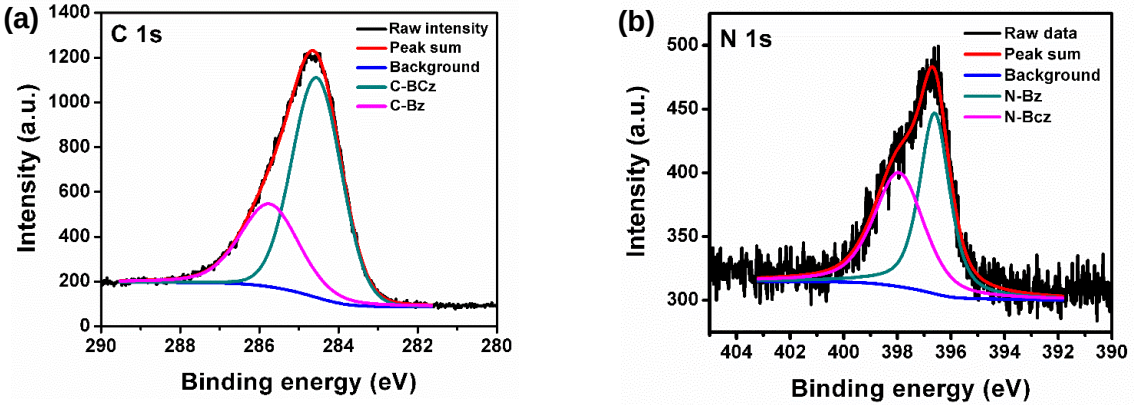

Fig. S3 The X-ray photoelectron spectroscopy (XPS) analysis of BCzBz for (a) C 1s, and (b) N 1s, respectively.

In the C 1s spectrum, we observed the peaks at 285.8 and 284.6 eV which were due to the sp^2-carbons of benzothiadiazole (Bz) and bicarbazole (BCz) units, respectively. In the N 1s spectrum, the peaks at 400.6 and 399.2 eV originated from the nitrogen atoms of bicarbazole and benzothiadiazole units, respectively present in the polymer (Fig. S3). The fitting parameter (χ^2) values for all the elements in the X-ray photoelectron spectra (XPS) of BCzBz were close to 1.

2.5.4 Energy dispersive X-ray (EDX) analysis coupled with high-resolution transmission electron microscopy (HRTEM):

The energy dispersive X-ray analysis (EDX) coupled with the high-resolution transmission electron microscopy (HRTEM) was carried out to check the Br content in the network polymer. We found 1.0 atom% (6.2 wt%) of Br content in BCzBz polymer (Fig. S4). The results suggested that some of the -Br functionalities remained unreacted during the polymerization. To get an idea about the degree of substitution of the bicarbazole monomer, we proposed an

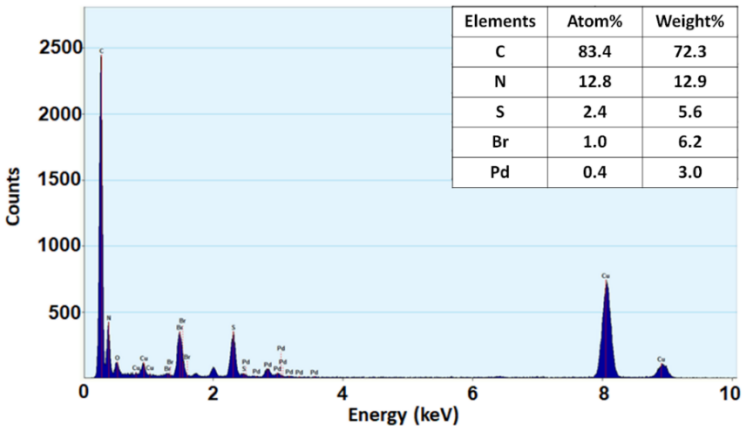

Fig. S4 Energy dispersive X-ray (EDX) analysis of BCzBz polymer coupled with high-resolution transmission electron microscopy; inset: tabular representation of different elements in atomic% and weight% present in the polymer. The peak for Cu in the EDX spectrum was due to the copper grid used for the sample analysis.

idealized model network structure based on the similarity of Br content following the protocols demonstrated in earlier literature.[1] The model structure (Fig. S5), consisting of 9 bicarbazole, 21 benzothiadiazole, and 5 unreacted Br units (molecular weight of 6183.25 g mol^{-1}), has the closest calculated Br-content (6.4 wt%) to that obtained from the EDX analysis. Hence, HRTEM-EDX analysis revealed that all bicarbazole monomers were unlikely to be tetrasubstituted.[2-4] The moderate specific BET surface area of BCzBz polymer (S_{BET} = 363 ± 33 m^2 g^{-1}) also ascertained a lower degree of cross-linking.

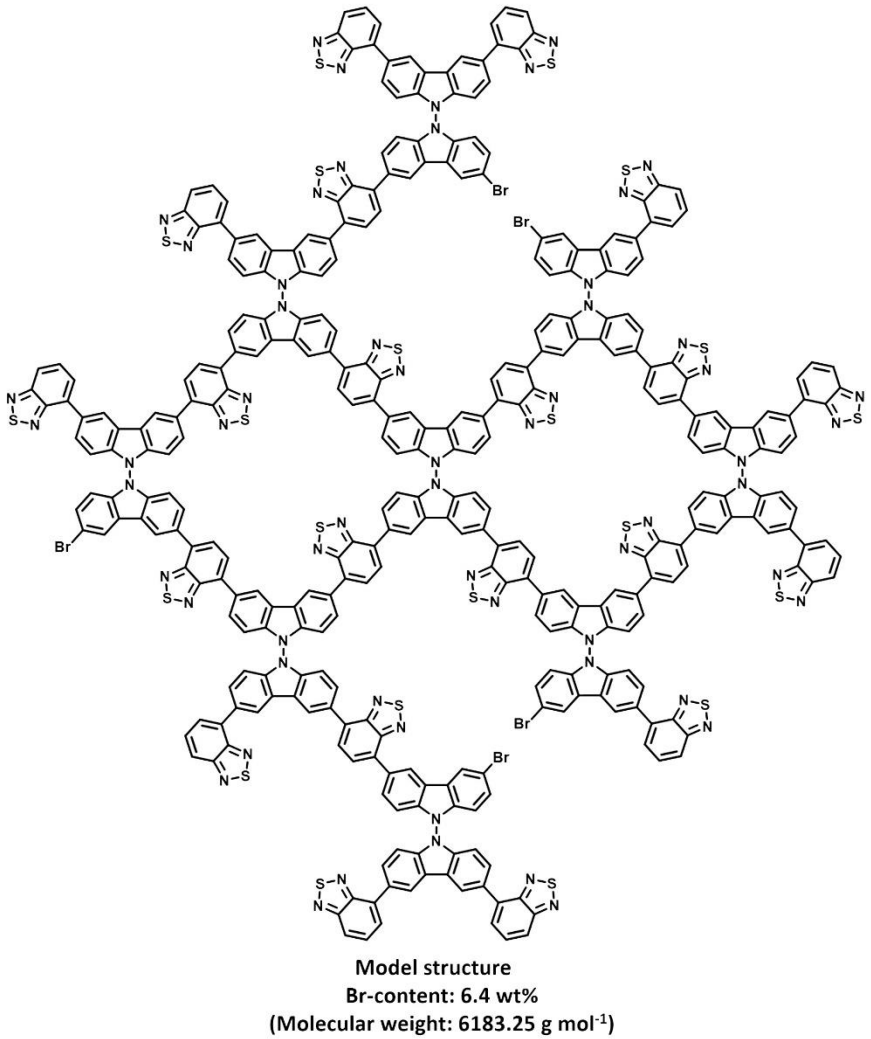

Fig. S5 Idealized model network structure considering the Br content obtained from the EDX analysis. Model structure: $C_{342}H_{161}Br_5N_{60}S_{21}$, Br: 6.4 wt%.

2.5.5 Field emission scanning electron microscopy (FESEM) analysis:

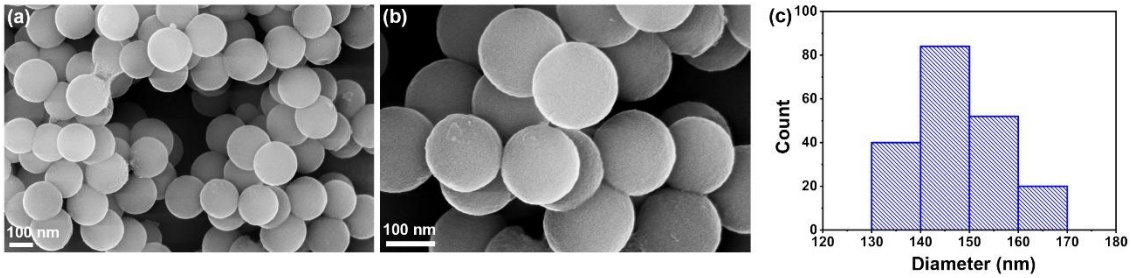

Fig. S6 (a, b) Field emission scanning electron microscopy (FESEM) images, and (c) particle size distribution of BCzBz polymer.

2.5.6 Atomic force microscopy (AFM) analysis:

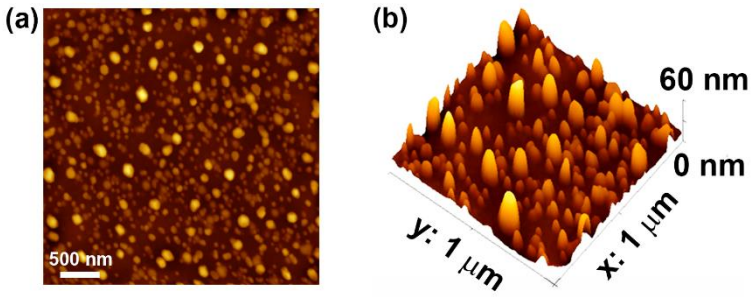

Fig. S7 Topographic atomic force microscopy (AFM) images of pristine BCzBz dispersion (a) along the X-Y plane and (b) the Z-axis.

2.5.7 Powder X-ray diffraction (PXRD) study: The broad PXRD profile signifies the amorphous nature of BCzBz polymer (Fig. S8).

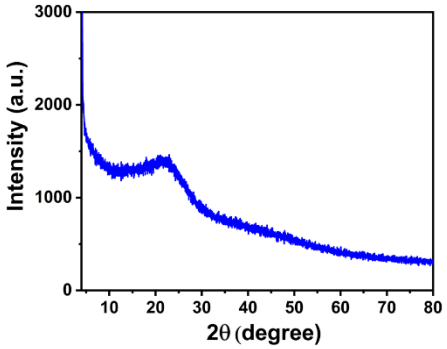

Fig. S8 Powder X-ray diffraction (PXRD) pattern of BCzBz.

2.5.8 Absorption spectra, Tauc plot of BCzBz:

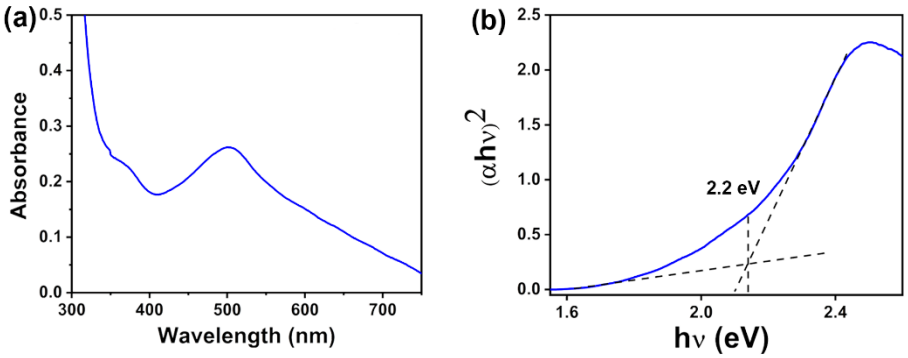

Fig. S9 (a) Absorption spectrum, and (b) Tauc plot of BCzBz dispersion in acetonitrile (1 mg mL^{-1}).

2.5.9 Cyclic voltammetry (CV) analysis:

The highest occupied molecular orbital (E_{HOMO}) and the lowest unoccupied molecular orbital (E_{LUMO}) energy levels of BCzBz were calculated using the following equations.[5]

$$E_g = E_{LUMO} - E_{HOMO} \qquad \text{(S2)}$$

$$E_{LUMO} = E_{red} \qquad \text{(S3)}$$

Here, E_g (2.2 V) and E_{red} (-0.94 V) are the optical band gap and reduction potential of BCzBz, respectively.

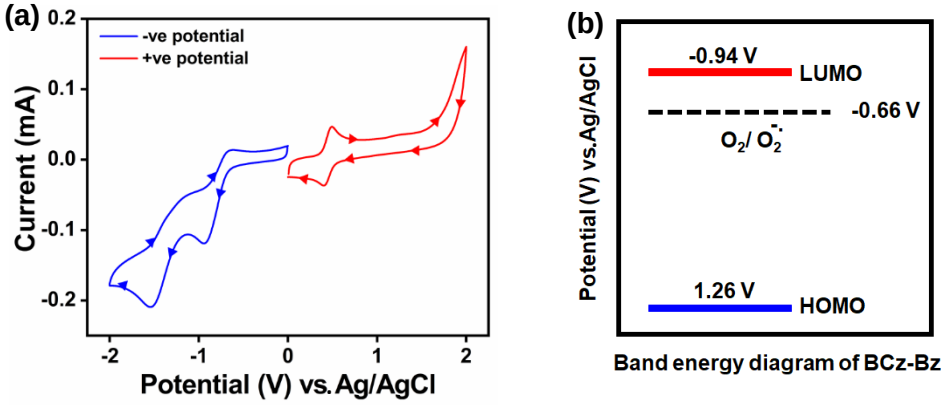

Fig. S10 (a) Cyclic voltammogram of BCzBz in acetonitrile; scan rate 100 mV s^{-1}, and (b) band energy diagram of BCzBz. Three electrode-cell system was used for the measurement [working electrode: BCzBz-coated glassy carbon electrode; counter electrode: Pt wire; reference electrode: Ag/AgCl (KCl, 3 M)]. Ferrocene-ferrocenium (Fc/Fc^+) was used as an internal standard.

III. Generation of reactive oxygen species

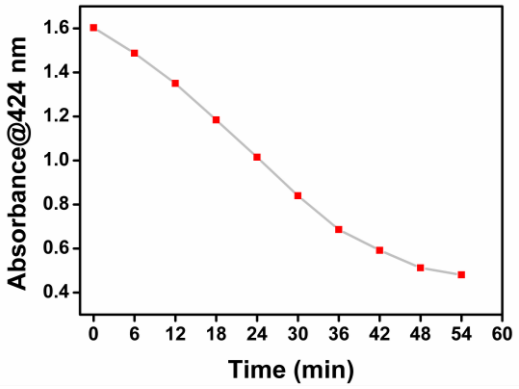

Fig. S11 Degradation of 1,3-diphenylisobenzofuran (DPBF; 50 μM, in 3 mL DMF) in the presence of BCzBz (300 μL, 1 mg mL^{-1} in DMF) with the variation of irradiation time at 530 nm using a green laser torch.

In a typical experimental procedure, the absorption spectra of a solution of 1,3-diphenylisobenzofuran (DPBF) and BCzBz in acetonitrile were monitored upon irradiation at 530 nm using a green laser torch for around 1 h with the acquisition of the spectrum every 6 min. The photochemical degradation of DPBF was observed only in the presence of BCzBz dispersion under photoirradiation (Fig. S11). The governing reaction that depicts the degradation of DPBF by $^1O_2$, generated upon photoirradiation of BCzBz is as follows (Scheme S2).[6]

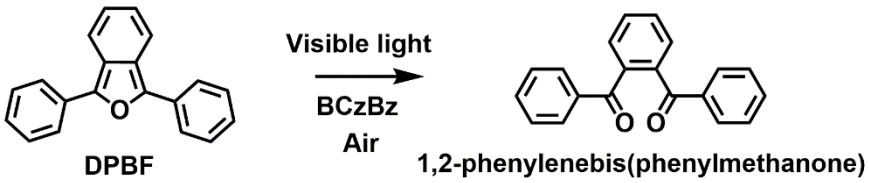

Scheme S2 Formation of 1,2-phenylenebis(phenylmethanone) due to the oxidation of 1,3-diphenylisobenzofuran (DPBF) by $^1O_2$ produced upon photoirradiation of BCzBz.

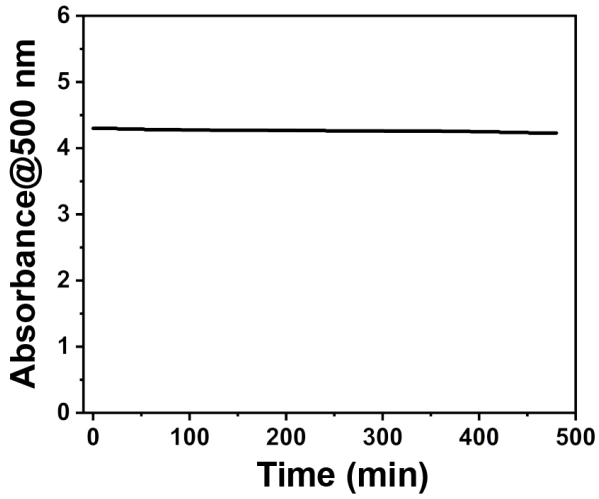

Fig. S12 Absorbance (@500 nm) vs. time profile (data acquisition in every 2 min) of BCzBz (1 mg/ 3 mL DMF) depicting the photostability of the polymer.

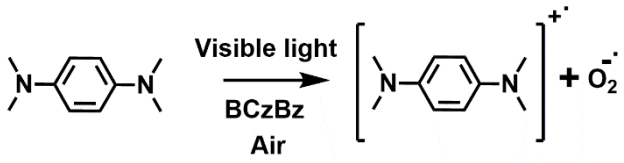

Scheme S3 Generation of cationic radical of *N*,*N*,*N′*,*N′*-tetramethyl-*p*-phenylenediamine (NTPD) and superoxide anion radicals upon photoirradiation of BCzBz.

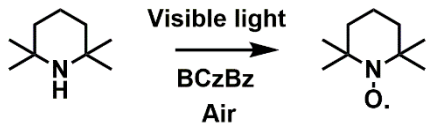

Scheme S4 Reaction scheme depicting formation of 2,2',6,6'-tetramethylpiperidine-1-oxyl (TEMPO) radical from 2,2',6,6'-tetramethylpiperidine (TEMP) upon photoirradiation of BCzBz.

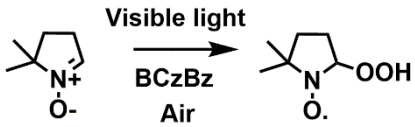

Scheme S5 Photochemical conversion of 5,5-dimethyl-1-pyrroline-*N*-oxide (DMPO) to oxidized DMPO by superoxide anion radicals, generated by BCzBz upon light irradiation.

IV. Intracellular ROS generation

2′,7′-dichlorodihydrofluorescin diacetate (DCHF-DA) was used as the indicator to probe BCzBz-mediated intracellular ROS generation. The conversion of DCHF-DA to 2′,7′-dichlorofluorescin (DCF) by ROS (produced by BCzBz upon light irradiation) led to the turn-on green fluorescence (Scheme S6).[7]

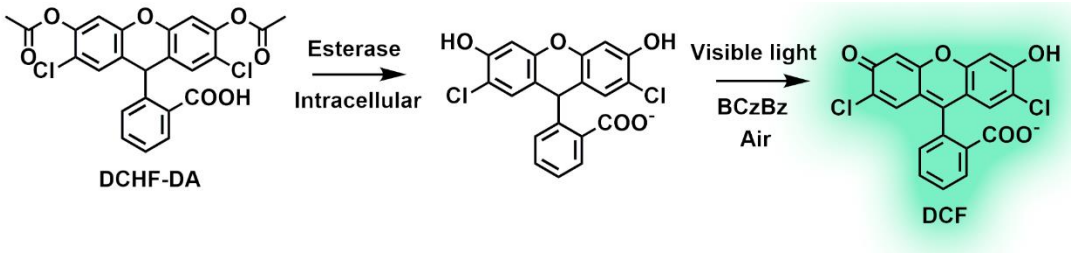

Scheme S6 Plausible mechanism for ROS-mediated conversion of non-fluorescent 2′,7′-dichlorodihydrofluorescin diacetate (DCHF-DA) to green fluorescent 2′,7′-dichlorofluorescin (DCF).

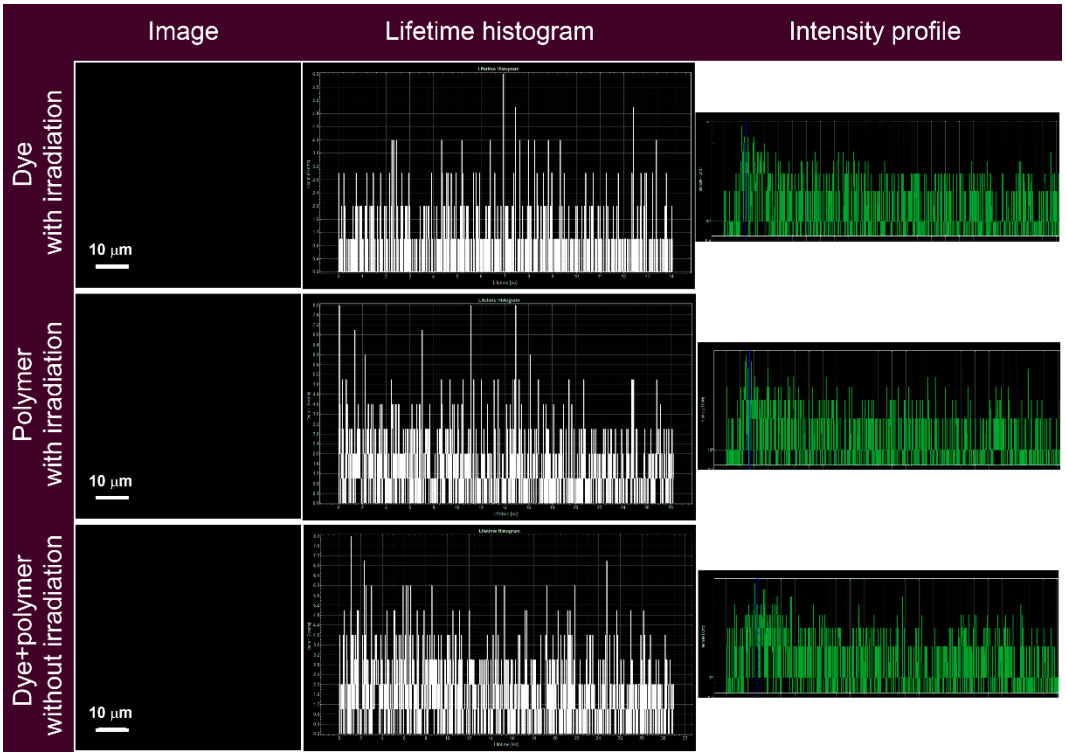

Fig. S13 Confocal laser scanning microscopy (CLSM) of HeLa cells incubated with 2′,7′-dichlorodihydrofluorescein diacetate (DCHF-DA; 10 μM) and its lifetime histograms, intensity profiles under different control conditions [top panel: cells were incubated with DCHF-DA (10 μM) with 530 nm photoirradiation for 5 min, middle panel: cells were incubated with BCzBz (30 μg mL^{-1}) with 530 nm photoirradiation for 5 min, and bottom panel: cells were incubated with DCHF-DA (10 μM) and BCzBz (30 μg mL^{-1}) without irradiation] depicting that the intracellular ROS-mediated fluorescence imaging using DCHF-DA was only possible in the presence of BCzBz under photoirradiation. Scale = 10 μm.

The confocal laser scanning microscopy (CLSM) and intensity vs. distance profiles of a particular region of interest (ROI; a single cell) in the CLSM images of HeLa cells were obtained using PicoQuant, MicroTime 200 instrument. All the measurements were carried out under similar conditions using the same laser source. The distance between the light source (530 nm laser torch) and Petri dish, and the area of irradiation was kept the same during all the measurements. To minimize the errors associated with different batches of cells used for the measurements and their shapes and sizes, we plotted the ratio of fluorescence intensities rather than the absolute value in Fig. 4d. Additionally, we considered the mean fluorescence intensity (MFI) over the maximum intensity value to get the ratio plot. Fig. 4d and Fig. S14 demonstrate a qualitative analysis to get an insight into the tunable intracellular ROS generation capability of BCzBz.

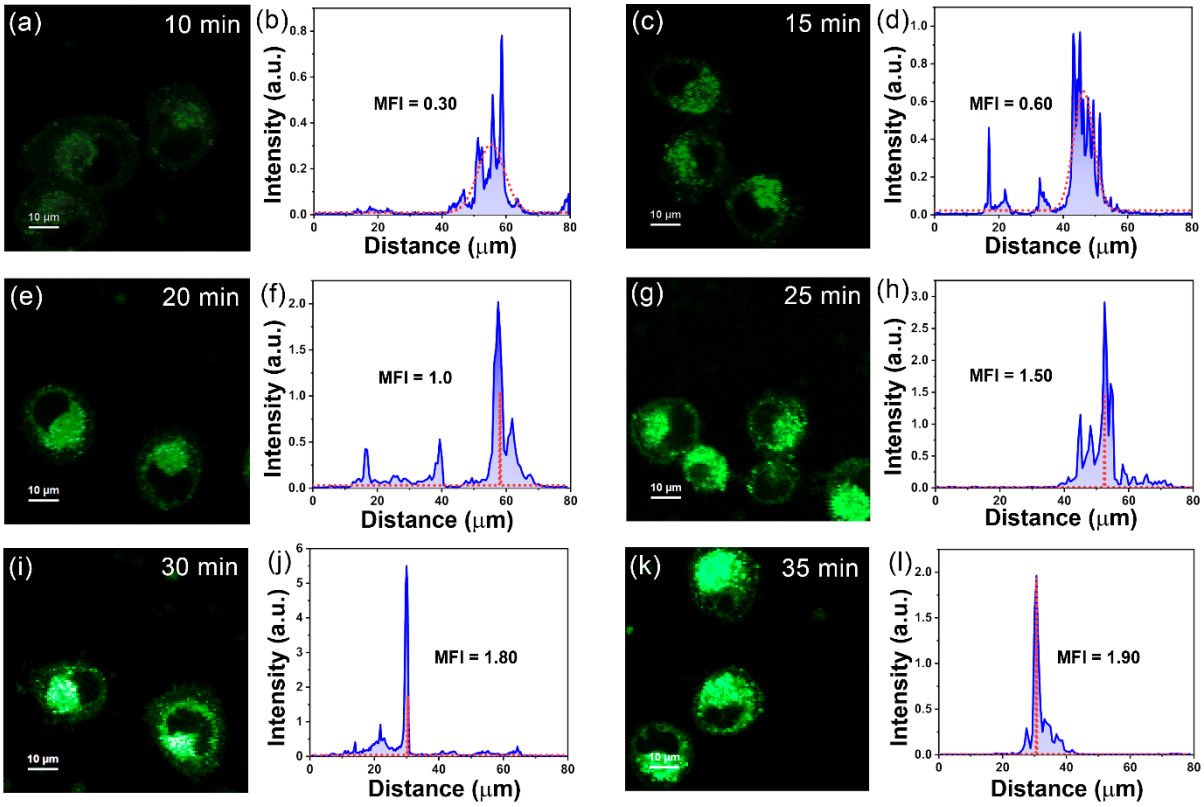

Fig. S14 Confocal laser scanning microscopy (CLSM) images (a, c, e, g, i, k; scale = 10 μm) and intensity vs. distance profiles (b, d, f, h, j, l) of a particular region of interest (ROI) in the CLSM images of HeLa cells [incubated with 2′,7′-dichlorodihydrofluorescein diacetate (10 μM) and BCzBz (30 μg mL^{-1})] with the variation of photoirradiation time (10 min to 35 min with 5 min intervals) depicting the tunable intracellular ROS generation capability of BCzBz. The increase in mean fluorescence intensity (MFI) with photoirradiation time is indicated (b, d, f, h, j, l).

V. Dose-dependent photo-induced cytotoxicity studies

We performed cytotoxicity studies in HeLa cells with the variation of polymer concentration and photoirradiation time independently to shed light on the dose-dependent photo-induced cytotoxicity of the materials.

In the first set of experiments, five different batches of HeLa cells were incubated with calcein AM (10 μM) and varying concentration of BCzBz (i) 10 μg mL^{-1}, (ii) 15 μg mL^{-1}, (iii) 20 μg mL^{-1}, (iv) 30 μg mL^{-1}, and (v) 40 μg mL^{-1}. All the different batches of incubated cells were photoirradiated at 530 nm for a constant irradiation time of 20 min. The bright green fluorescence was observed from the cells which were incubated with calcein AM and respectively, 10, 15, and 20 μg mL^{-1} BCzBz (Fig. S15a-c). In contrast, no fluorescence was noticed for the cells incubated with the dye and BCzBz (30 and 40 μg mL^{-1}) upon irradiation at 530 nm for 20 min (Fig. S15d, S15e, Fig. 5d, main text). The results implied that the cell death occurred due to the greater abundance of ROS in the presence of a higher concentration of BCzBz under photoirradiation (Fig. S15d, S15e). Similarly, five different batches of HeLa cells were incubated with propidium iodide (PI: 10 μM) and varying concentration of BCzBz (i) 10 μg mL^{-1}, (ii) 15 μg mL^{-1}, (iii) 20 μg mL^{-1}, (iv) 30 μg mL^{-1}, and (v) 40 μg mL^{-1}. The red fluorescence due to the cell death was only observed when the cells were incubated with PI and higher concentrations of BCzBz polymer (20, 30, 40 μg mL^{-1}) under photoirradiation at 530 nm (Fig. S15f-j, Fig. 5h, main text).

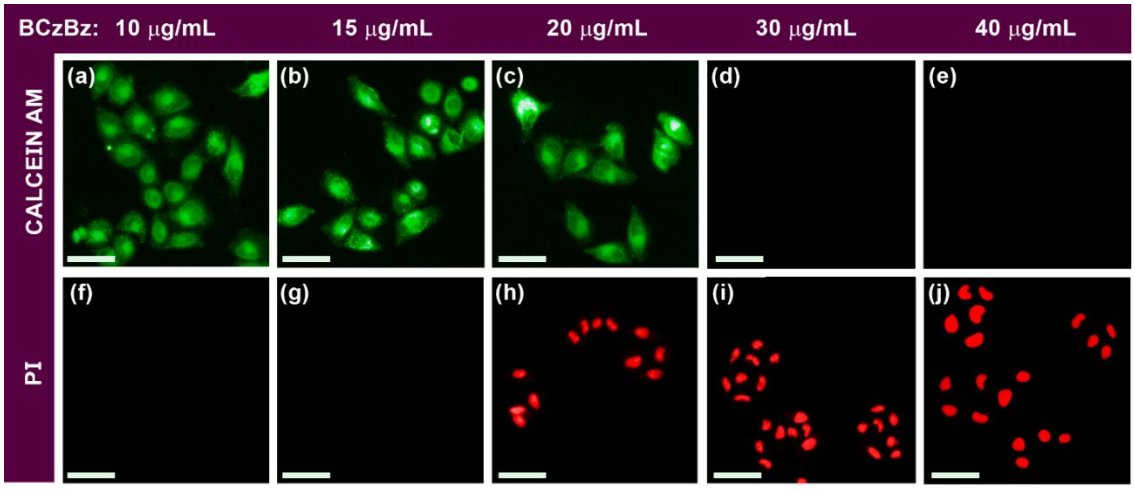

Fig. S15 Fluorescence microscopy images of HeLa cells; upper panel: cells stained with calcein AM (10 μM), live cell staining dye and varying concentration of BCzBz (a) 10 μg mL^{-1}, (b) 15 μg mL^{-1}, (c) 20 μg mL^{-1}, (d) 30 μg mL^{-1}, and (e) 40 μg mL^{-1}; GFP filter (green channel, λ_{ex} = 450-490 nm, λ_{em} = 500-550 nm). Lower panel: cells stained with propidium iodide (PI: 10 μM), dead cell staining dye and varying concentration of BCzBz (f) 10 μg mL^{-1}, (g) 15 μg mL^{-1}, (h) 20 μg mL^{-1}, (i) 30 μg mL^{-1}, and (j) 40 μg mL^{-1}; DsReD filter (red channel, λ_{ex} = 538-562 nm, λ_{em} = 570-640 nm). All the different batches of incubated cells were photoirradiated at 530 nm for a constant irradiation time of 20 min. Scale = 20 μm.

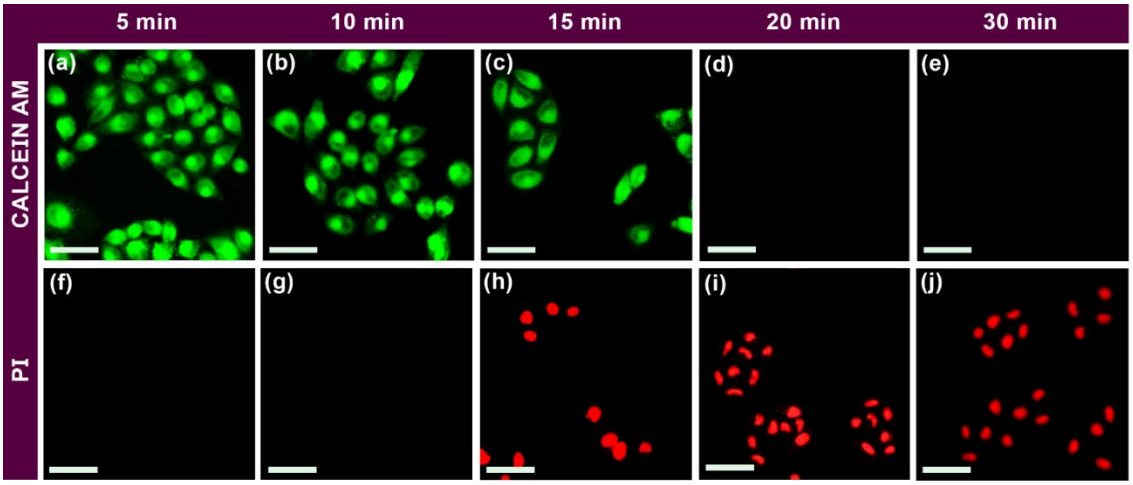

Fig. S16 Fluorescence microscopy images of HeLa cells; upper panel: cells stained with calcein AM (10 µM), live cell staining dye and BCzBz (30 µg mL^{-1}), and photoirradiated at 530 nm with the variation of photoirradiation time, (a) 5 min, (b) 10 min, (c) 15 min, (d) 20 min, and (e) 30 min; GFP filter (green channel, λ_{ex} = 450-490 nm, λ_{em} = 500-550 nm). Lower panel: cells stained with propidium iodide (PI: 10 µM), dead cell staining dye and BCzBz (30 µg mL^{-1}), and photoirradiated at 530 nm with varying photoirradiation time, (f) 5 min, (g) 10 min, (h) 15 min, (i) 20 min, and (j) 30 min; DsReD filter (red channel, λ_{ex} = 538-562 nm, λ_{em} = 570-640 nm). Scale = 20 µm.

In another set of experiments, five different batches of HeLa cells were incubated with BCzBz (30 µg mL^{-1}) and calcein AM (10 µM) and photoirradiated at 530 nm for different time duration. The bright green fluorescence was observed from the cells, which were photoirradiated for 5, 10, and 15 min (Fig. S16a-c). In contrast, no fluorescence was noticed for the cells which were irradiated for 20 and 30 min (Fig. S16d, S16e, Fig. 5d, main text). The results implied that the cell death occurred due to the greater abundance of ROS due to the higher photoirradiation time. Similarly, five different batches of HeLa cells were incubated with BCzBz (30 µg mL^{-1}) and propidium iodide (PI: 10 µM). The red fluorescence due to the cell death was only observed when the cells were photoirradiated at 530 nm for 15, 20, and 30 min (Fig. S16f-j, Fig. 5h, main text).

Future scope of BCzBz: We demonstrated that the pristine BCzBz dispersion could be used for probing the generation of the intracellular reactive oxygen species (ROS) through the ratiometric mean fluorescence intensity (MFI) vs. time of irradiation profile (Fig. S14). Hence, we can evaluate the extent of ROS generation in different cells under specific physiological conditions.[8] However, it is pertinent to envisage the targeted delivery of BCzBz, e.g., for photodynamic therapy.

Post-synthetic modifications, either through covalent approaches or tuning of the noncovalent intermolecular interactions, are the two distinct design strategies for the development of cancer cell-specific molecular materials.[8,9] A diverse range of ligands were

reported to functionalize the nanoprobes for the specific targeting of the cancer cell membrane receptors, e.g., folic acid.[9] As revealed from the EDX analysis, BCzBz possesses unreacted bromo functionalities, which can be converted to boronic acid through Suzuki coupling. Subsequently, boronic acid residues can be substituted by folic acid via the standard EDC-NHS coupling route.[10] Such folic acid functionalized BCzBz nanoparticles are likely to be specific to the cancer cells. On the other hand, the surface modification of BCzBz can also be achieved through the noncovalent approaches. The BCzBz nanoparticles can be encapsulated into the hydrophobic micellar core through a miniemulsion technique using an anionic surfactant, e.g., sodium dodecyl sulfate (SDS). An electrostatic assembly of negatively charged nanoparticles with a folate-conjugated cationic triblock copolymer will be specific for the folate receptor over-expressing cancer cells.[11] Some of these avenues are going to be explored in our laboratory.

VI. Comparative analysis

Table S2. A comparative account of *N*,*N*'-bicarbazole-benzothiadiazole-based conjugated porous organic polymer (BCzBz) developed in the present study with some of the most significant materials reported for intracellular reactive oxygen species (ROS) generation based on porous organic materials, conjugated linear organic polymers, nanocomposites, and small organic molecules.

System	Abs. Max.	Photostability	Intracellular ROS generation	Live-dead cell assay	Time-dependent intracellular ROS generation	Ref.
BCzBz	500 nm	Yes	Yes	Yes	Yes	Present work
Porous organic materials						
Corrole-based COF (TPAPC-COF)	Broad (covering UV, Visible, NIR)	Not shown	No	Yes	No	*Angew. Chem. Int. Ed.*, 2020, **59**, 4354.[12]
BODIPY decorated nanoscale COFs	400-800 nm broad spectra	Yes	Yes	Yes	Yes	*iScience*, 2019, **14**, 180.[13]
Conjugated linear organic polymers						
Conjugated linear polymer, CP4	520 nm	Yes	Yes	Yes	No	*Chem*, 2018, **4**, 1937.[14]
Conjugated polymer nanoparticles, PFVBT	502 nm	Yes	Yes	No	No	*Small*, 2017, **13**, 1602807.[15]
Nanocomposites						
MOF@POP-PEG nanocomposite, HUC-PEG	400-700 nm; Broad absorption band	Yes	Yes	Yes	No	*Biomaterials*, 2020, **235**, 119792.[16]
COF+BSA nanocomposite, COF-B	400-800 nm broad spectra	Yes	No	Yes	No	*Mater. Chem. Front.*, 2020, **4**, 2346.[17]
Metal organic framework, PS@MOF-199 NPs	480 nm	Yes	Yes	No	No	*ACS Nano*, 2019, **13**, 6879.[18]
Metal organic framework, F127-PS@MIL-100	505 nm	Not shown	Yes	Yes	No	*Adv. Funct. Mater.*, 2018, **28**, 1707519.[19]

Metal-organic framework (MOF)@POP composite, (UNM)	430 nm	Yes	Yes	Yes	No	*Chem. Mater*., 2017, **29**, 2374.[20]
Small organic molecules						
Tetraphenylethylene-based small organic molecule	420 nm	Yes	No	No	No	*Chem. Mater*., 2020, **32**, 4681.[21]
Seleno-rosamine dye	520 nm	Not shown	No	Yes	No	*J. Am. Chem. Soc*., 2017, **139**, 13713.[22]
Substituted rhodol dye	430 nm	Not shown	Yes	Yes	No	*Chem. Sci*., 2016, **7**, 1862.[23]

VII. References

1. A. Laybourn, R. Dawson, R. Clowes, T. Hasell, A. I. Cooper, Y. Z. Khimyak and D. J. Adams, *Polym. Chem.*, 2014, **5**, 6325.
2. R. S. Sprick, A. Thomas and U. Scherf, *Polym. Chem.*, 2010, **1**, 283.
3. E. Preis, C. Widling, U. Scherf, S. Patil, G. Brunklaus, J. Schmidt and A. Thomas, *Polym. Chem.*, 2011, **2**, 2186.
4. G. Liu, Y. Wang, C. Shen, Z. Ju and D. Yuan, *J. Mater. Chem. A*, 2015, **3**, 3051.
5. W. Huang, B. C. Ma, D. Wang, Z. J. Wang, R. Li, L. Wang, K. Landfester and K. A. I. Zhang, *J. Mater. Chem. A*, 2017, **5**, 3792.
6. X. Ding and B. Han, *Angew. Chem. Int. Ed.*, 2015, **54**, 6536.
7. X. Chen, Z. Zhong, Z. Xu, L. Chen and Y. Wang, *Free Radic. Res.*, 2010, **44**, 587.
8. S. Liu, G. Feng, B. Z. Tang and B. Liu, *Chem. Sci.*, 2021, **12**, 6488.
9. K. Ulbrich, K. Holá, V. Šubr, A. Bakandritsos, J. Tuček and R. Zbořil, *Chem. Rev.*, 2016, **116**, 5338.
10. S. Mitra, H. S. Sasmal, T. Kundu, S. Kandambeth, K. Illath, D. D. Díaz and R. Banerjee, *J. Am. Chem. Soc.*, 2017, **139**, 4513.
11. L. Liu, A. Patra, U. Scherf and T. Kissel, *Macromol. Biosci*., 2012, **12**, 1384.
12. Y. Zhao, W. Dai, Y. Peng, Z. Niu, Q. Sun, C. Shan, H. Yang, G. Verma, L. Wojtas, D. Yuan, Z. Zhang, H. Dong, X. Zhang, B. Zhang, Y, Feng and S. Ma, *Angew. Chem. Int. Ed.*, 2020, **59**, 4354.
13. Q. Guan, D. Fu, Y. Li, X. Kong, Z. Wei, W. Li, S. Zhang and Y. Dong, *iScience*, 2019, **14**, 180.
14. W. Wu, D. Mao, S. Xu, Kenry, F. Hu, X. Li, D. Kong and B. Liu, *Chem*, 2018, **4**, 1937.
15. G. Feng, Y. Fang, J. Liu, J. Geng, D. Ding and B. Liu, *Small*, 2017, **13**, 1602807.
16. X. Zheng, L. Wang, Y. Guan, Q. Pei, J. Jiang and Z. Xie, *Biomaterials*, 2020, **235**, 119792.
17. T. Sun, R. Xia, J. Zhou, X. Zheng, S. Liu and Z. Xie, *Mater. Chem. Front.*, 2020, **4**, 2346.
18. Y. Wang, W. Wu, J. Liu, P. N. Manghnani, F. Hu, D. Ma, C. Teh, B. Wang and B. Liu, *ACS Nano*, 2019, **13**, 6879.
19. F. Hu, D. Mao, Kenry, Y. Wang, W. Wu, D. Zhao, D. Kong and B. Liu, *Adv. Funct. Mater.*, 2018, **28**, 1707519.
20. X. Zheng, L. Wang, Q. Pei, S. He, S. Liu and Z. Xie, *Chem. Mater.*, 2017, **29**, 2374.
21. B. Guo, M. Wu, Q. Shi, T. Dai, S. Xu, J. Jiang and B. Liu, *Chem. Mater*., 2020, **32**, 4681.
22. W. Piao, K. Hanaoka, T. Fujisawa, S. Takeuchi, T. Komatsu, T. Ueno, T. Terai, T. Tahara, T. Nagano and Y. Urano, *J. Am. Chem. Soc*., 2017, **139**, 13713.
23. Y. Yuan, C. Zhang, S. Xua and B. Liu, *Chem. Sci*., 2016, **7**, 1862.

VIII. ^{1}H, ^{13}C NMR spectra

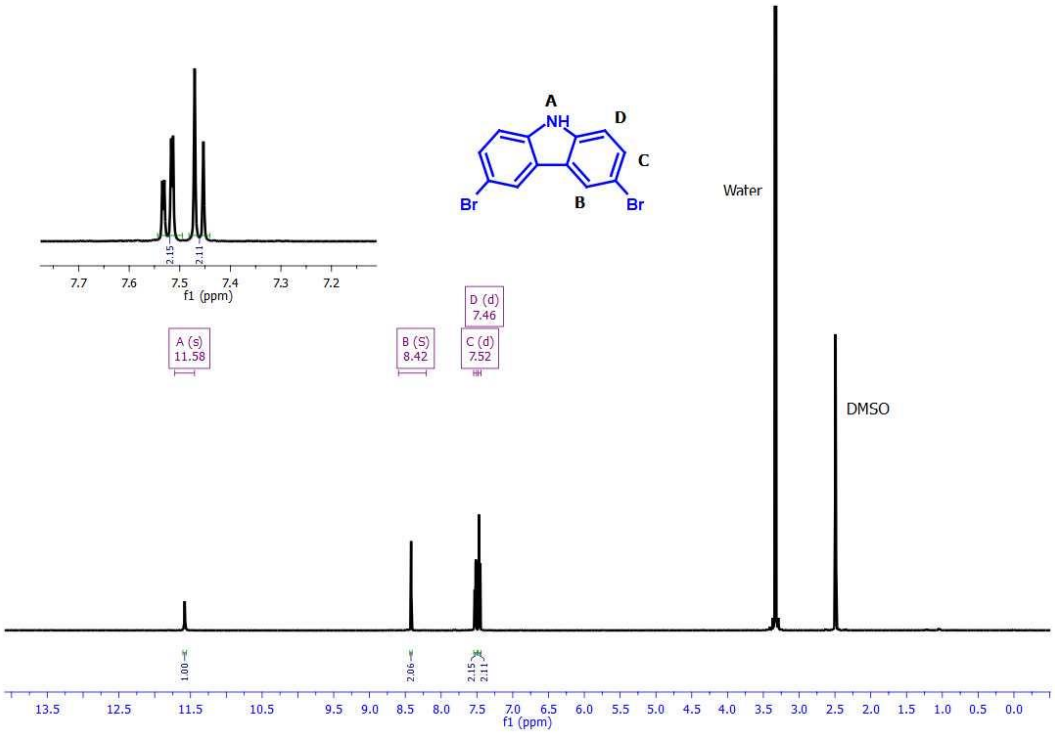

Fig. S17 ^{1}H NMR spectrum of 3,6-dibromo-9*H*-carbazole.

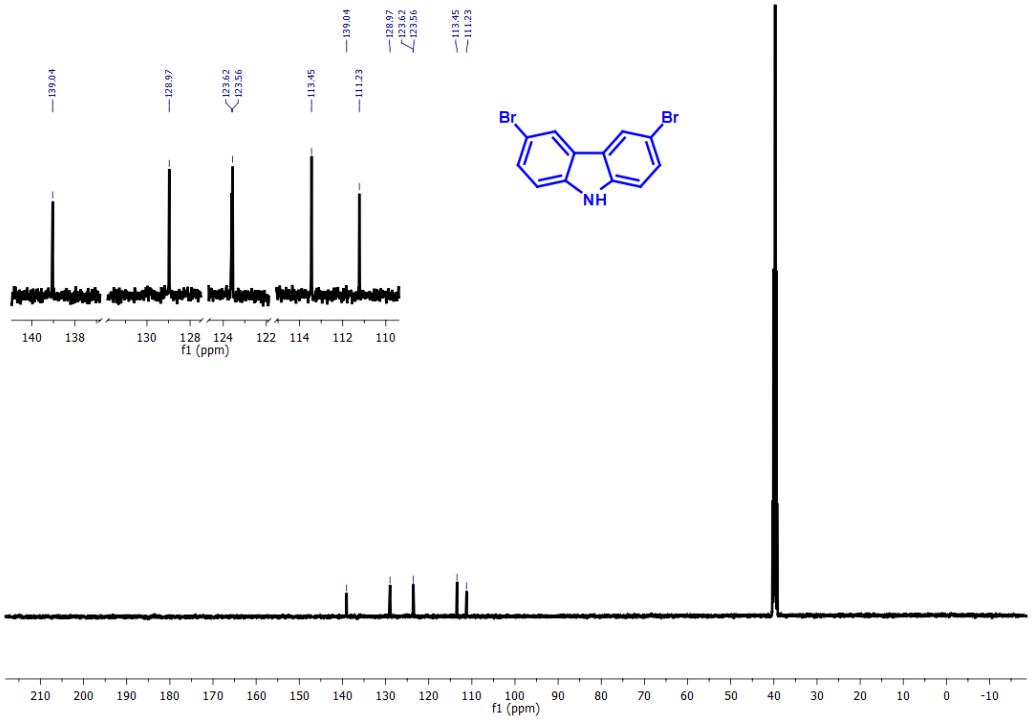

Fig. S18 ^{13}C NMR spectrum of 3,6-dibromo-9*H*-carbazole.

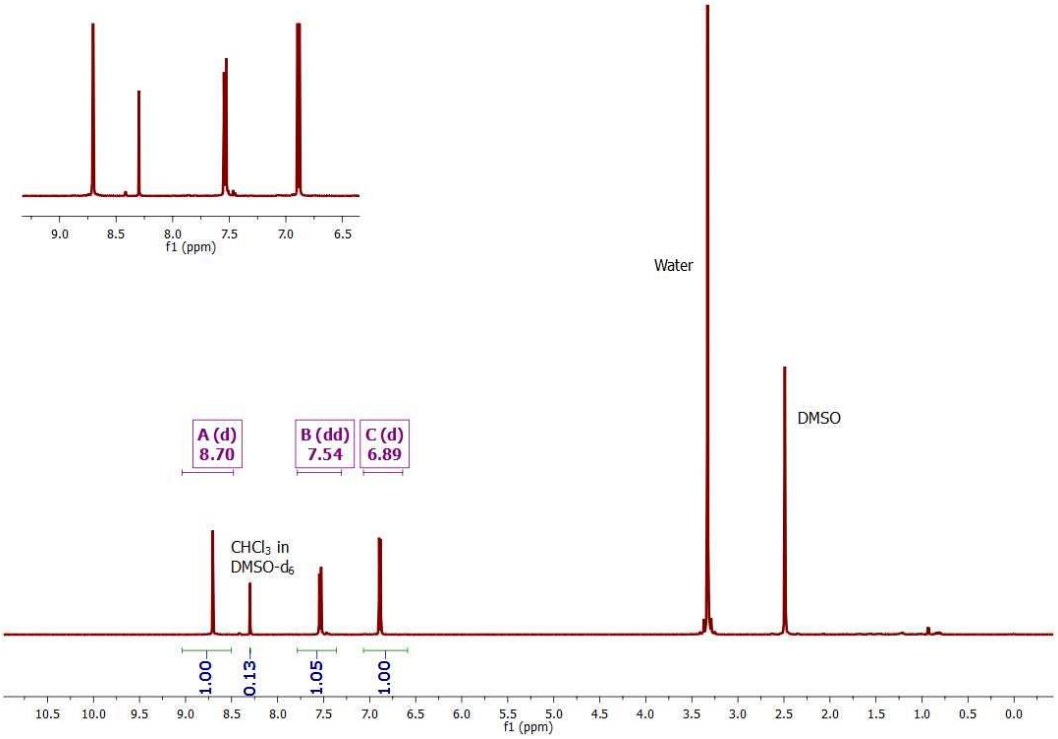

Fig. S19 ^{1}H NMR spectrum of 3,3',6,6'-tetrabromo-*N*,*N'*-bicarbazole.

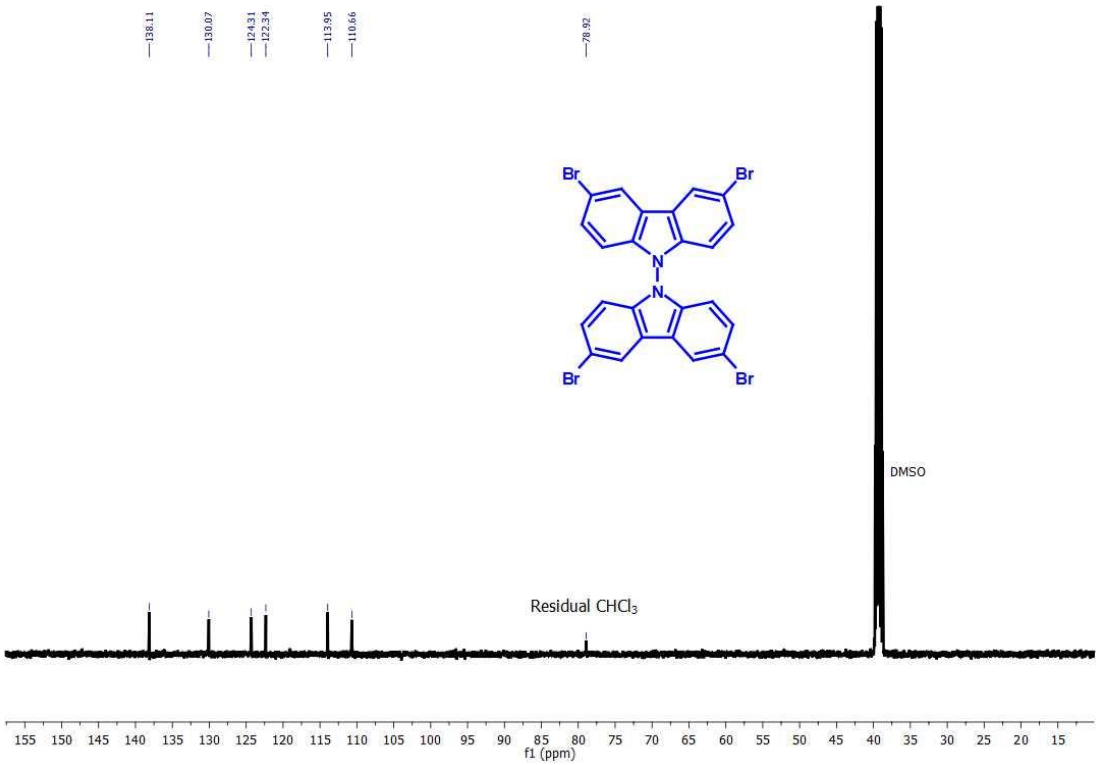

Fig. S20 ^{13}C NMR spectrum of 3,3',6,6'-tetrabromo-*N*,*N'*-bicarbazole.